第36卷第1期
2017年2月

红外与毫米波学报
J. Infrared Millim. Waves

Vol. 36, No. 1
February, 2017

文章编号：1001－9014(2017)01－0001－06

DOI:10.11972/j.issn.1001－9014.2017.01.001

Influence of various Cu contents on the microstructure of Cu(In,Ga)Se_2 thin films

SUN Lei[1,2], MA Jian-Hua[1*], YAO Niang-Juan[1,2], HUANG Zhi-Ming[1], CHU Jun-Hao[1]

(1. National Laboratory for Infrared Physics, Shanghai Institute of Technical Physics, Chinese Academy of Sciences, Shanghai 200083, China;
2. Shanghai Center for Photovoltaics, Shanghai 200083, China)

Abstract: The influence of different Cu contents (Cu/(Ga + In) = 0.748 ~ 0.982) on the microstructure of Cu(In,Ga)Se_2 (CIGS) thin films was reported. The CIGS thin films were grown via a two-step process including DC sputtering deposition of metallic precursor and following selenization. Presence of a series of chalcopyrite diffraction peaks in the X-Ray diffraction (XRD) patterns confirms the existence of chalcopyrite CIGS (CH-CIGS) phase in these CIGS films. The Raman spectra indicate that as the Cu content increases from low to high, the CIGS film sequentially goes through three phase regimes: coexistence of OVC and CH-CIGS phase, single CH-CIGS phase and coexistence of Cu_xSe and CH-CIGS phase. Moreover, the full width at half maximum of CIGS Raman peaks changes with Cu/(Ga + In) and reaches its minimum near Cu/(Ga + In) = 0.9 due to better crystallinity and less disorder. Some empirical FWHM-Cu/(Ga + In) relationships were also observed. These results show that Raman spectroscopy is more sensitive to the microstructure of CIGS film than XRD, and can be used for preliminary estimation of the crystal phases and Cu content of CIGS film in a fast and non-destructive way.

Key words: CIGS thin films, Cu content, microstructure, raman spectra
PACS: 88.40.jn, 68.55.Nq, 78.30.Fs

铜含量变化对 Cu(In,Ga)Se_2 薄膜微结构的影响

孙 雷[1,2], 马建华[1*], 姚娘娟[1,2], 黄志明[1], 褚君浩[1]

(1. 中国科学院上海技术物理研究所 红外物理国家重点实验室,上海 200083;
2. 上海太阳能电池研究与发展中心, 上海 200083)

摘要:报道了不同的铜含量(Cu/(Ga + In) = 0.748 ~ 0.982)对 Cu(In,Ga)Se_2(CIGS)薄膜微结构的影响. 文章中的CIGS薄膜采用磁控溅射金属预置层后硒化的方法制备,其X射线衍射谱(XRD)中一系列黄铜矿结构CIGS(CH-CIGS)相的衍射峰确认了CH-CIGS相的存在. 对CIGS薄膜拉曼光谱的分析表明,随着铜含量的上升,CIGS薄膜经历了CH-CIGS和有序缺陷化合物(OVC)混合相、CH-CIGS单相、CH-CIGS和Cu_xSe混合相三种状态. 进一步的分析显示,CIGS薄膜拉曼峰的半高宽随铜含量变化,并在Cu/(Ga + In) = 0.9附近时达到最小值,这说明此时CIGS薄膜具有更好的结晶度和更少的无序性. 此外还得到了CIGS薄膜拉曼峰半高宽与铜含量的经验关系公式. 这些研究表明拉曼光谱能比XRD更加灵敏地探测CIGS薄膜的微结构,可望作为一种无损和快速测量方法,用于对CIGS薄膜晶相和铜含量的初步估计.

关 键 词:CIGS薄膜;铜含量;微结构;拉曼光谱

中图分类号:TM914.4 +2　　**文献标识码**:A

Received date: 2016-06-16, **revised date**: 2016-09-30　　**收稿日期**:2016-06-16, **修回日期**:2016-09-30

Foundation items: Supported by National Natural Science Foundation of China (NSFC) (61006092), and the key incubation project of Shanghai Institute of Technical Physics (Chinese Academy of Science)

Biography: SUN Lei (1983-), male, Yunnan, China. Doctor candidate. Research area involves photovoltaic materials and devices. E-mail: ksml@163.com
* **Corresponding author**: E-mail: mjhling@mail.sitp.ac.cn

Introduction

Chalcopyrite (CH) polycrystalline semiconductors such as $CuInSe_2$ (CIS) and $Cu(In,Ga)Se_2$ (CIGS) are promising absorber materials for high efficiency and low cost thin film solar cells. The recorded efficiency of 22.3% has been achieved at laboratory[1-2]. The optical and electrical properties of CIGS film are strongly related to chemical composition and crystal phase composition [3-6]. Deviations from stoichiometry can lead to intrinsic defects, such as vacancies and antisites, which dominate the electrical properties of CIGS. The Secondary phases, like Cu_xSe, ordered vacancy compound (OVC) and CuAu-ordered CIGS, form in CIGS films with varying composition. CIGS films with Cu-poor composition are usually used to avoid the formation of highly conductive Cu_xSe phase which is harmful to the efficiency of device[4]. On the other hand, the presence of Cu-poor OVC in the surface region of CIGS films is assumed to be beneficial for device performance [6].

X-Ray diffraction and Raman spectroscopy are both important methods to characterize the microstructure and crystallinity of thin film. The XRD presents the overall information of crystalline phase, but is not sensitive to the secondary phases like OVC and CuAu-ordered CIGS due to the overlap of diffraction peaks[7-8]. Meanwhile, Raman spectroscopy is a nondestructive measurement method and very sensitive to near-surface microstructure and crystal quality. Since the Cu content of high-performance CIGS solar cells is in a range of $0.8 < Cu/(Ga+In) < 0.95$[9-11], we performed XRD and Raman analysis of the microstructure evolution of CIGS thin films with Cu/(Ga + In) ratios ranging from 0.748 to 0.982 in this work. Our results have the potential to be used for non-destructive estimation of the crystal phases and Cu content of CIGS film.

1 Experiments

CIGS films of this work were grown on Mo-coated soda-lime glass (SLG) slides by two-step process consisting of sputtering of metallic precursor and subsequent selenization. The Mo-layer was deposited by DC magnetron sputtering and about 0.8 μm thick. The Cu-In-Ga (CIG) precursors were deposited in a sandwich structure of CuGa/In/CuGa at 200 centigrade. CuGa target (atomic ratio of Cu/Ga = 75/25) and In target were used in turn, and the thickness of precursor is approximate 0.8 μm. The CIG precursors were then selenized with a 2-step reaction temperature profile in a graphite box containing Se powder. Firstly, the precursors were heated to 270 centigrade and kept for 10min to form copper selenide and indium selenide compounds. Secondly, the precursors were heated to 500 centigrade and kept for 30min to form $Cu(In,Ga)Se_2$ chalcopyrite phase. The composition and thickness of CIGS films were determined by X-ray fluorescence (XRF) analysis with SHIMADZU EDX - 7000 which generates the X-ray radiation with a Rh tube. Scanning electron microscopy (SEM) of PHILIPS XL30 was used to examine the morphology of CIGS films. The crystal phases of CIGS films were investigated at room temperature by Bruker D8 ADVANCE X-ray diffractometer with Cu K radiation in mode. All diffraction peaks were identified by comparing with JCPDS data. Raman measurements were performed at room temperature using TII Nanofinder 30 micro-Raman system in backscattering configuration. The wavelength of excitation laser is 532 nm and the diameter of laser spot is less than 1 μm (100X objective of the microscope). The excitation power of laser beam used in our experiment was kept at 1mW to prevent damage to the samples and thermal effects in the spectra. The penetration depth of this laser in CIGS films is around 100 nm.

2 Results and Discussion

Table 1 Composition of CIGS films on Mo-coated soda-lime glass measured by XRF. All composition ratios are atomic ratios

表 1 由 XRF 测量的 CIGS 薄膜组份比例,所有组份比例均为原子比. CIGS 薄膜生长在镀 Mo 钠钙玻璃衬底上

Cu/(Ga + In)	Ga/(Ga + In)	Se/(Cu + Ga + In)
0.748	0.166	1.006
0.806	0.179	0.998
0.824	0.180	1.004
0.843	0.191	1.004
0.858	0.190	1.008
0.883	0.196	0.992
0.928	0.208	0.993
0.934	0.211	0.997
0.982	0.216	0.991

The detailed overall compositions of all samples measured by XRF are listed in Table 1. The Ga/(Ga + In) ratios (all composition ratios in this paper are atomic ratios) are within the range of 0.16 ~ 0.22 which does not bring meaningful influence to the optoelectronic properties of CIGS films[12-14]. In order to eliminate the influence of different Se contents, we hold the Se/metal ratios of the samples around 1 within the range of 0.01. The thicknesses of the CIGS films in this work are about 2μm, which is also determined by XRF.

The SEM images in Fig. 1 show the surface morphology of four samples selected from low Cu content to high Cu content in Table 1. It is widely accepted that Cu content has a great influence in shaping the morphology and microstructure of CIGS film[4-5]. The grain boundaries are blurry in (a) and (d) but unambiguous in (b) and (c). However, the change of grain size over Cu content is not visible in Fig. 1, and it is hard to estimate the crystallinity based on the SEM images. The XRD patterns of these four samples, shown in Fig. 2, clearly exhibit a series of diffraction peaks from chalcopyrite CIGS (CH-CIGS) phase (PDF#35-1102-CuInGaSe) including three major peaks such as (112), (220/204) and (116/312) as well as other minor peaks such as (101), (103), (211) and (213). These diffraction peaks confirm the presence of CH-CIGS phase in our CIGS films. Apart from these CH-CIGS based peaks and Mo (110) peak, no other peaks form secondary phase like OVC phase or Cu_xSe phase can be observed. All CH-CIGS

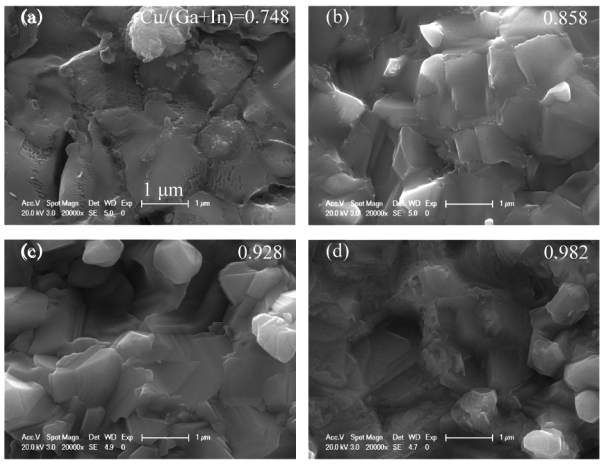

Fig. 1　Surface SEM images of CIGS thin films. From (a) to (d), the Cu/(Ga + In) ratios of CIGS thin films are 0.748, 0.858, 0.928 and 0.982, respectively

图 1　CIGS 薄膜的表面 SEM 图像,(a)到(d)分别对应 Cu/(Ga + In)比例为 0.748,0.858,0.928,0.982 的 CIGS 薄膜

based peaks, from the bottom to the top in Fig. 2, shift about to higher as a consequence of the increase of Ga content[8] in our samples (shown in Table 1). However, the changes of full width at half maximum (FWHM) and relative intensity with varying Cu content are not noticeable.

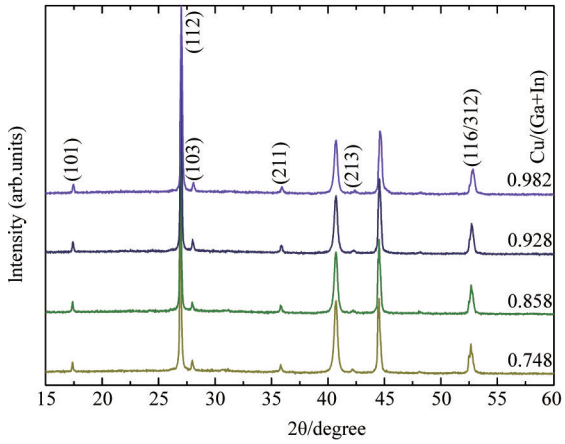

Fig. 2　XRD patterns of CIGS thin films grown on Mo/SLG as a function of Cu/(Ga + In) ratio. All samples show a series of XRD peaks from CH-CIGS phase (PDF# 35-1102-CuInGaSe)

图 2　Mo/SLG 衬底上不同 Cu/(Ga + In)比例的 CIGS 薄膜的 XRD 衍射图样. 所有样品都显示了一组来自于黄铜矿 CIGS 相的衍射峰(PDF#35-1102-CuInGaSe)

We conducted Raman spectra measurements of a series CIGS films with different Cu contents to investigate the relationship between Cu content and crystal phase composition of CIGS film as shown in Fig. 3. All spectra were measured at room temperature, and normalized to the dominant vibration mode at 174 cm^{-1}. Since the polycrystalline CIGS films were examined by a micro-Raman system, each spectrum in Fig. 3 was obtained by scanning ten positions in line with 10μm step and then averaging the raw data from these ten positions. For the CIGS films with Cu/(Ga + In) around 0.9, the Raman peak at 174 cm^{-1}, corresponding to A_1 mode of CH-CIGS phase[13], dominates the Raman spectra in Fig. 3. Several weaker peaks from CH-CIGS phase are also clearly shown in Fig. 3 : the peaks at 64 cm^{-1} and 72 cm^{-1} are assigned to mode and mode[13-14]; the peaks at 214 cm^{-1} and 231 cm^{-1} are identified with E mode and E/B_2 mode[13-14]. These vibration modes clearly confirm the pure CH-CIGS phase in these CIGS films. As the Cu/(Ga + In) increases to nearly 1, the Cu_xSe phase, which is an indispensable intermediate phase during the selenization, begins to precipitate and turn the CIGS film into double phase including Cu_xSe and CH-CIGS phase. The Cu-richest sample (Cu/(Ga + In) = 0.982) exhibits a Raman peak at 258 cm^{-1} which is known as A_1 mode of Cu_xSe compounds like CuSe or Cu_2Se [15-16]. The Cu_xSe phase deteriorates the performance of final devices because it has high p-type conductivity and produces shunt paths which lowers the open circuit voltage of solar cells[17-19]. On the other hand, when the Cu/(Ga + In) decreases to below 0.8, complex defects consisting of Cu vacancies and In_Cu antisites ($2V_Cu^- + In_Cu^{2+}$) are randomly introduced into the lattice and form the OVC

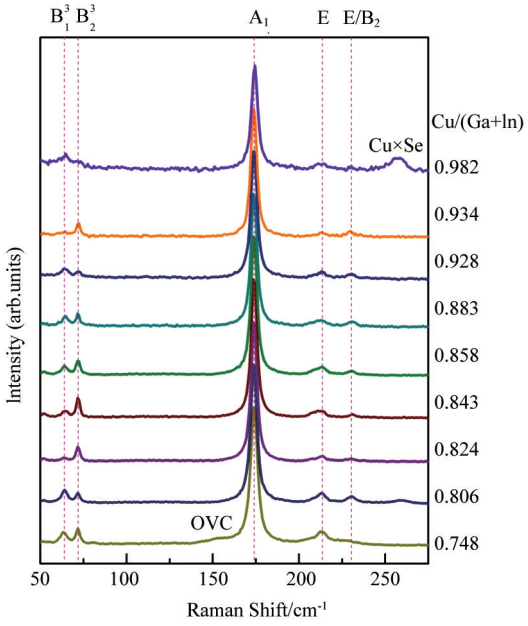

Fig. 3　Raman spectra of CIGS thin films with different Cu/(Ga + In) ratios measured at room temperature. All spectra are normalized to the CIGS A_1 peak. The sample with Cu/(Ga + In) = 0.748 shows a broad shoulder from OVC phase at around 154 cm^{-1}, and the sample with Cu/(Ga + In) = 0.982 exhibits a peak at around 258 cm^{-1} corresponding to Cu_xSe phase

图 3　室温下不同 Cu/(Ga + In)比例的 CIGS 薄膜的拉曼光谱,所有光谱都通过 CIGS 的 A_1 峰进行归一化. Cu/(Ga + In)比例为 0.748 的样品在 154 cm^{-1}处显示出来自于 OVC 相的肩峰,Cu/(Ga + In)比例为 0.982 的样品在 258 cm^{-1}处显示出来自于 Cu_xSe 相的峰

phases like $Cu(In,Ga)_3Se_5$ or $Cu_2(In,Ga)_4Se_7$ which have similar structure of chalcopyrite-type. For the Cu-poorest sample ($Cu/(Ga+In)=0.748$), a broad shoulder appears around 154 cm^{-1} which is known as the main vibration mode from OVC phase[15,17] (the details are shown in Fig. 4).

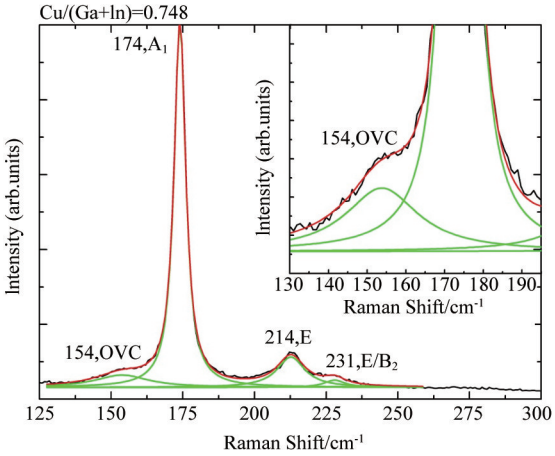

Fig. 4 The Raman spectrum of Cu-poorest sample with $Cu/(Ga+In)=0.748$. The spectrum was fitted with four Lorentzian functions. The green curves are the Lorentzian fitted peaks for four Raman peaks. The red curve, coinciding well with the Raman spectrum, is the summation of the four Lorentzian fitted peaks. The inset is the zoomed view of the broad shoulder of OVC phase

图4 贫铜样品拉曼光谱的 Lorentzian 函数拟合,样品的 $Cu/(Ga+In)$ 比例为 0.748. 绿色曲线是四个独立的 Lorentzian 函数,红色曲线为四个 Lorentzian 函数相加后的拟合曲线. 从图中可以看出,红色拟合曲线和拉曼光谱符合得很好. 插图是 OVC 相引起的肩峰的放大显示图

The OVC induced broad shoulder of Raman spectrum with $Cu/(Ga+In)=0.748$ is not very clear in Fig. 3, so that we fitted this spectrum with four Lorentzian functions in Fig. 4. The spectral line shape of Raman spectra is Lorentzian function which can be represented as

$$I = \frac{1}{1+(\omega-\omega_0)^2/(w/2)^2}, \quad (1)$$

where I is the normalized intensity, ω is the Raman shift, ω_0 is the position of Raman peak and w is the FWHM. The four Lorentzian fitted peaks (the green curves in Fig. 4) correspond to the four Raman modes, three of which (174, 214, 231 cm^{-1}) are assigned to CH phase[13-14], and the remaining one (154 cm^{-1}) is assigned to OVC phase[15,17]. This fitted result corroborates the coexistence of CH phase and OVC phase in the Cu-poor CIGS film. The complex defects ($2V_{Cu}^{-} + In_{Cu}^{2+}$) in the OVC phase are stable, electrically neutral and have little effect on the electrical properties of CIGS[20-21]. The OVC phase in the surface region of the CIGS absorbers is assumed to improve the performance of the solar cells. This is because the OVC has a higher band gap than CIGS, which leads to a better band alignment at the buffer/absorber interface [22] and the formation of an isomeric junction between p-CIGS absorber and n-OVC, replacing the heterojunction at the CdS/CIGS interface[3]. The above analysis of Raman spectra indicates the evolution of crystal phase composition with varying Cu content. As the Cu content increases from low to high, the CIGS film sequentially goes through three phase regimes: coexistence of OVC and CH-CIGS phase, single CH-CIGS phase and coexistence of Cu_xSe and CH-CIGS phase. Therefore, we can approximately estimate the Cu content range of CIGS film from the shape of Raman spectra.

We also use Lorentzian function to fit Raman spectra of all samples to get the positions and FWHMs of Raman peaks. The positions of CIGS Raman peaks do not shift obviously, possibly because Ga accumulates at the back-side of CIGS film[23] which leads to a slight Ga content variation at the near-surface region where Raman measurements investigate. Otherwise, FWHMs of CIGS Raman peaks exhibit some interesting changes. Figure 5 shows the dependency of the FWHM of Raman peaks on the copper content. The FWHM is inversely proportional to the lifetime of elementary excitation (e. g. phonon) and is a measure of the crystallinity[20]. The FWHM of A_1 peak with different Cu contents is below 5 cm^{-1} (Fig. 5a) which is relatively small compared with the literature reports[5,8] and suggests a high crystal quality of our CIGS films. The A_1 peak is broadened for Cu-poor and Cu-rich films and reaches its FWHM minimum near $Cu/(Ga+In)=0.9$ (Fig. 5a), which is the optimal range of best devices reported[9-11]. This is because the secondary phases, like OVC phase in Cu-poor film and Cu_xSe phase in Cu-rich film, introduce defects and reduced crystallinity into the CIGS films[5]. Similar trend of the relationship between the FWHM and the Cu content can be seen for peak at 72 cm^{-1} in Fig. 5b and peak at 64 cm^{-1} in Fig. 5c. We fitted the FWHM data in Fig. 5 with quadratic polynomials to derive the empirical formulas of the three peaks as follows:

$$FWHM_{174} = 34.1 - 67.7x + 38.2x^2 \quad (2)$$

$$FWHM_{72} = 58.9 - 135x + 80.9x^2 \quad (3)$$

$$FWHM_{64} = 176 - 421x + 258x^2 \quad (4)$$

where x is the $Cu/(Ga+In)$ ratio. The smaller error of FWHM of A_1 peak makes Eq. (2) more confident than Eq. (3) and Eq. (4). It is useful to evaluate the CIGS absorber soon after its deposition during the fabrication process of solar cell. Raman spectroscopy is more sensitive to crystal phase and crystal quality than SEM and XRD. Although the Raman spectroscopy only provides near-surface information, the depth distribution of chemical and crystalline composition does not change obviously in the different samples which are deposited by the same process. Besides, there is not apparent variation of the depth distribution of Cu content in the CIGS film[23]. Therefore, the above Raman spectra analysis and the empirical FWHM-$Cu/(Ga+In)$ relationships are hopeful to be used for preliminary estimation of the crystal phases and Cu content of CIGS film in a fast and non-destructive way.

3 Conclusion

In summary, CIGS films with different $Cu/(Ga+In)$ ratios (from 0.748 to 0.982) were studied by care-

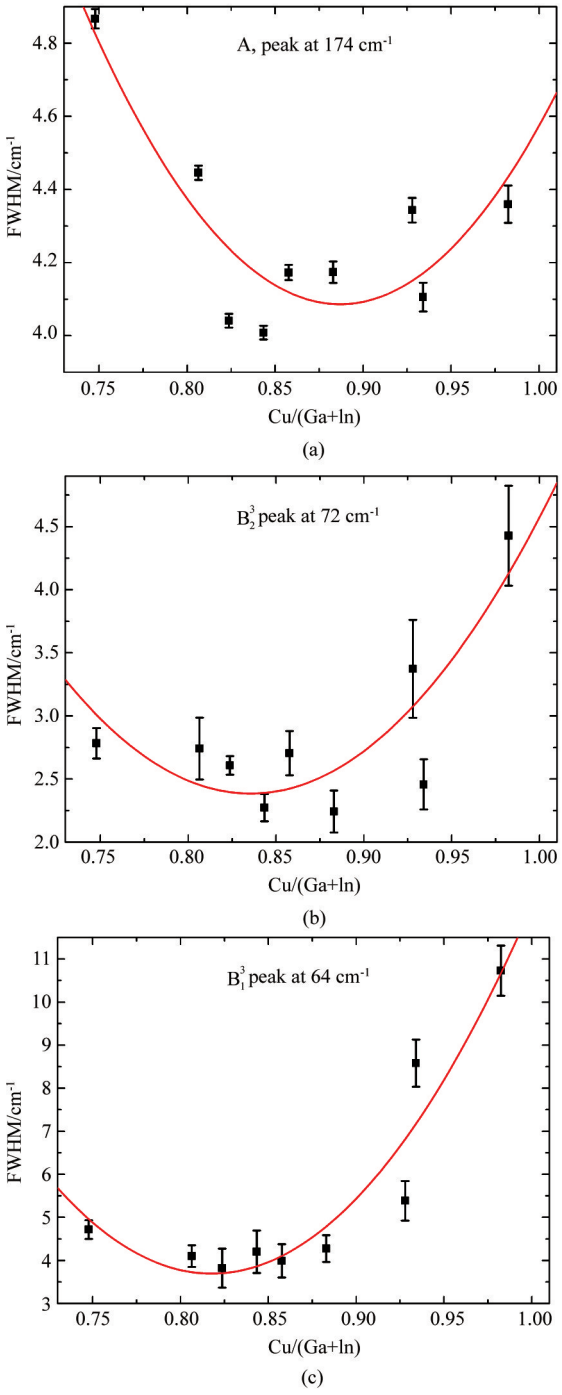

Fig. 5　The relationships between the FWHM of Raman peaks and the Cu/(Ga + In) ratio. The red curves are fitted results. The figures are: (a) A_1 peak at 174 cm^{-1}, (b) peak at 72 cm^{-1}, (c) peak at 64 cm^{-1}

图 5　拉曼峰的 FWHM 和 Cu/(Ga + In)比例的关系图,红色曲线是拟合曲线. 图片分别对应:(a)在 174 cm^{-1} 处的 A_1 峰;(b)在 72 cm^{-1} 处的峰;(c)在 64 cm^{-1} 处的峰

ful Raman spectra and XRD analysis in this paper. These films were deposited by two-step process consisting of sputtering of metallic precursor and subsequent selenization. The XRD patterns confirm the chalcopyrite CIGS phase in films, while the Raman spectra exhibit the formation of chalcopyrite phase as well as some secondary phases like OVC phase in Cu-poor film and Cu_xSe phase in Cu-rich film. Some empirical relationships between the FWHM of Raman peaks and Cu/(Ga + In) are derived from the Raman spectra. It can be concluded that Raman spectroscopy is more sensitive to the crystal phase and quality of CIGS film than XRD. Our results could be used to approximately estimate the crystal phases and Cu content of CIGS film without destruction.

References

[1] Friedlmeier T M, Jackson P, Bauer A, *et al.* Improved Photocurrent in Cu(In,Ga)Se_2 Solar Cells: From 20.8% to 21.7% Efficiency with CdS Buffer and 21.0% Cd-Free [J]. *IEEE Journal of Photovoltaics*, 2015, 5: 1487.

[2] Solar Frontier Achieves World Record Thin-Film Solar Cell Efficiency: 22.3%, http://www.solar-frontier.com/eng/news/2015/C051171.html.

[3] Siebentritt S, Gutay L, Regesch D, *et al.* Why do we make Cu(In,Ga)Se_2 solar cells non-stoichiometric [J]. *Solar Energy Materials & Solar Cells*, 2013, **119**: 18.

[4] Virtuani A, Lotter E, Powalla M, *et al.* Influence of Cu content on electronic transport and shunting behavior of Cu(In,Ga)Se_2 solar cells [J]. *Journal of Applied Physics*, 2006, **99**: 014906.

[5] Witte W, Kniese R, Powalla M, Raman investigations of Cu(In,Ga)Se_2 thin films with various copper contents [J]. *Thin Solid Films*, 2008, **517**: 867.

[6] Insignares-Cuello C, Broussillou C, Bermúdez V, *et al.* Raman scattering analysis of electrodeposited Cu(In,Ga)Se_2 solar cells: Impact of ordered vacancy compounds on cell efficiency [J]. *Applied Physics Letters*, 2014, **105**: 021905.

[7] Ramdani O, Guillemoles J F, Lincot D, *et al.* One-step electrodeposited $CuInSe_2$ thin films studied by Raman spectroscopy [J]. *Thin Solid Films*, 2007, **515**: 5909.

[8] Jeong A R, Jo W, Song M, *et al.* Crystalline ordered states of $CuIn_{1-x}Ga_xSe2$ (x = 0, 0.3, and 1.0) thin-films on different substrates investigated by Raman scattering spectroscopy [J]. *Materials Chemistry and Physics*, 2012, **134**: 1030.

[9] Powalla M, Jackson P, Witte W, *et al.* High-efficiency Cu(In,Ga)Se_2 cells and modules [J]. *Solar Energy Materials & Solar Cells*, 2013, **119**: 51.

[10] Repins I, Contreras M A, Egaas B, *et al.* 19·9%-efficient ZnO/CdS/$CuInGaSe_2$ solar cell with 81·2% fill factor [J]. *Progress in Photovoltaics*, 2008, **16**: 235.

[11] Contreras M A, Romero M J, Noufi R, Characterization of Cu(In,Ga)Se_2 materials used in record performance solar cells [J]. *Thin Solid Films*, 2006, **51**: 511.

[12] Choi I, Raman spectroscopy of $CuIn_{1-x}Ga_xSe_2$ for in-situ monitoring of the composition ratio [J]. *Thin Solid Films*, 2011, **519**: 4390.

[13] Álvarez-García J, Barcones B, Pérez-Rodríguez A, *et al.* Vibrational and crystalline properties of polymorphic $CuInC_2$ (C = Se, S) chalcogenides [J]. *Physical Review B*, 2005, **71**: 054303.

[14] Roy S, Gaha P, Kundu S N, *et al.* Characterization of Cu(In,Ga)Se_2 films by Raman scattering [J]. *Materials Chemistry and Physics*, 2002, **73**: 24.

[15] Fontané X, Izquierdo-Roca V, Calvo-Barrio L, *et al.* In-depth resolved Raman scattering analysis of secondary phases in Cu-poor $CuInSe_2$ based thin films [J]. *Applied Physics Letters*, 2009, **95**: 121907.

[16] Minceva-Sukarova B, Najdoski M, Grozdanov I, *et al.* Raman spectra of thin solid films of some metal sulfides [J]. *Journal of Molecular Structure*, 1997, 410-411: 267.

(下转第 29 页)

4 Conclusion

Based on the coupled wave theory and the mode-matching method, a waveguide system to generate HE_{11} mode was designed and analyzed in this paper. The calculations and simulations showed that the system performed well in transforming from TE_{01} to HE_{11} mode. The cold tests to the waveguide system confirmed that the system we designed has great performance in mode conversion.

References

[1] Thumm M, Jacobs A, Sorolla Ayza M. Design of short high-power TE_{11}-HE_{11} mode converters in highly overmoded corrugated waveguides [J]. *IEEE Transactions on Microwave Theory & Techniques*, 1991, **39**(2):301 - 309.

[2] Denisov G G, Kulygin M L. Numerical Simulation of Waveguide TE_{01}-TE_{11} Mode Converter Using FDTD Method [J]. *Journal of Infrared, Millimeter, and Terahertz Waves*, 2005, **26**(3):341 - 361.

[3] Lyneis C, Benitez J, Hodgkinson A, *et al*. A mode converter to generate a Gaussian-like mode for injection into the VENUS electron cyclotron resonance ion source [J]. *Review of Scientific Instruments*, 2014, **85**(2):02A932 - 02A932.

[4] LI Hong-Fu, MANFRED THUMM. Mode conversion due to curvature in corrugated waveguides [J]. *International Journal of Electronics*, 1991, **71**(2):333 - 347.

[5] LI Hong-Fu, MANFRED THUMM. Mode coupling in corrugated waveguides with varying wall impedance and diameter change [J]. *International Journal of Electronics*, 1991, **71**(5):827 - 844.

[6] NIU Xin-Jian, ZHU Xian-Neng, LIU Ying-Hui, *et al*. Study of Ka-band TE_{01} to TE_{11} Mode Converters with Parallel Input and Output Waveguides [J]. *Journal of Infrared Millimeter and Terahertz Waves*, 2014, **35**(2):179 - 186.

[7] NIU Xin-Jian, LEI Chao-Jun, Liu Ying-Hui, *et al*. A Study on 94 GHz Low-Voltage, Low-Current Gyrotron [J]. *IEEE Transactions On Electron Devices*, 2013, **60**(11): 3907 - 3912.

[8] NIU Xin-Jian, LI Hong-Fu, XIE Zhong-Lian. Analysis of 8 mm high power TE_{01} TM_{11} mode converter in overmoded waveguide [C]. Bei-Jing: ICMMT 2002.

(上接 5 页)

[17] Xu C M, Xu X L, Xu J, *et al*. Composition dependence of the Raman A_1 mode and additional mode in tetragonal Cu-In-Se thin films [J]. *Semiconductor Science and Technology*, 2004, **19**: 1201.

[18] Han J, Liao C, Jiang T, *et al*. Investigation of copper indium gallium selenide material growth by selenization of metallic precursors [J]. *Journal of Crystal Growth*, 2013, **382**: 56.

[19] Turcu M., Pakma O, Rau U, Interdependence of absorber composition and recombination mechanism in $Cu(In,Ga)(Se,S)_2$ heterojunction solar cells [J]. *Applied Physics Letters*, 2002, **80**: 2598.

[20] Dieing T, Hollricher O, Toporski J, *Confocal Raman Microscopy* [M]. Berlin Heidelberg, Springer-Verlag, 2010: 73 - 74.

[21] Márquez R, Rincón C, Defect physics of the ordered defect compound $CuIn_3Se_5$ [J]. *Solar Energy Materials & Solar Cells*, 2002, **71**: 19.

[22] Dullweber T, Hanna G, Rau U, *et al*. A new approach to high-efficiency solar cells by band gap grading in $Cu(In,Ga)Se_2$ chalcopyrite semiconductors [J]. *Solar Energy Materials & Solar Cells*, 2001, **67**: 145.

[23] Liao K H, Su C Y, Ding Y T, Effects of Ga accumulation on the microstructure of $Cu(In_{1-x},Ga_x)Se_2$ thin films during selenization [J]. *Journal of Alloys and Compounds*, 2013, **581**: 250.